# Design and Discovery of 6-[(3S,4S)-4-Methyl-1-(pyrimidin-2-ylmethyl)pyrrolidin-3-yl]-1-(tetrahydro-2H-pyran-4-yl)-1,5-dihydro-4H-pyrazolo[3,4-d]pyrimidin-4-one (PF-04447943), a Selective Brain Penetrant PDE9A Inhibitor for the Treatment of Cognitive Disorders

Patrick R. Verhoest,* Kari R. Fonseca, Xinjun Hou, Caroline Proulx-LaFrance, Michael Corman, Christopher J. Helal, Michelle M. Claffey, Jamison B. Tuttle, Karen J. Coffman, Shenpinq Liu, Frederick Nelson, Robin J. Kleiman, Frank S. Menniti, Christopher J. Schmidt, Michelle Vanase-Frawley, and Spiros Liras

Neuroscience Medicinal Chemistry, Pfizer World Wide Research and Development, 700 Main Street, Cambridge, Massachusetts 02139, United States

Ⓢ *Supporting Information*

ABSTRACT: 6-[(3S,4S)-4-Methyl-1-(pyrimidin-2-ylmethyl)pyrrolidin-3-yl]-1-(tetrahydro-2H-pyran-4-yl)-1,5-dihydro-4H-pyrazolo[3,4-d]pyrimidin-4-one (PF-04447943) is a novel PDE9A inhibitor identified using parallel synthetic chemistry and structure-based drug design (SBDD) and has advanced into clinical trials. Selectivity for PDE9A over other PDE family members was achieved by targeting key residue differences between the PDE9A and PDE1C catalytic site. The physicochemical properties of the series were optimized to provide excellent in vitro and in vivo pharmacokinetics properties in multiple species including humans. It has been reported to elevate central cGMP levels in the brain and CSF of rodents. In addition, it exhibits procognitive activity in several rodent models and synaptic stabilization in an amyloid precursor protein (APP) transgenic mouse model. Recent disclosures from clinical trials confirm that it is well tolerated in humans and elevates cGMP in cerebral spinal fluid of healthy volunteers, confirming that it is a quality pharmacological tool for testing clinical hypotheses in disease states associated with impairment of cGMP signaling or cognition.
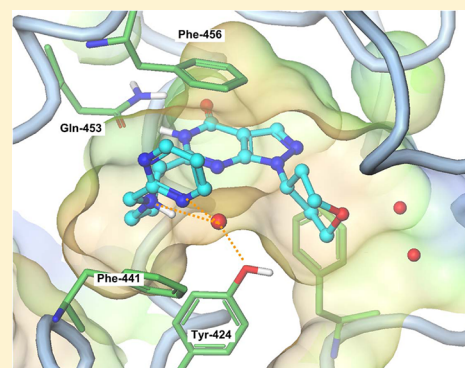
INTRODUCTION

Phosphodiesterase (PDE) enzymes catalyze the hydrolysis of cGMP and cAMP, which are ubiquitously utilized second messengers for intracellular signaling cascades invoked by a wide variety of biological stimuli and are of particular functional importance in the central nervous system (CNS).[1] There are 21 PDE genes subclassified into 11 different families (PDE1−11). Each family member is characterized by a unique cellular and subcellular distribution, distinct regulatory domains, enzyme kinetics, and substrate affinity for cGMP, cAMP, or both.[2] cGMP-specific PDEs include PDEs 5, 6, and 9, while cAMP-specific PDEs include 4, 7, and 8 and the PDEs 1, 2, 3, 10, and 11 are dual-substrate PDEs. The ability to potentiate specific cyclic nucleotide cascades by selectively targeting specific PDEs has led to the development of multiple drugs from this class of enzyme inhibitors. To date, inhibitors for PDEs 3, 4, and 5 have been approved for conditions that include congestive heart failure, chronic obstructive pulmonary disease, erectile dysfunction, and pulmonary hypertension.[3−5]

Although PDEs have proven to be druggable targets, achieving high selectivity among the gene family can be challenging and is desirable for adequate safety profiles, since unwanted PDE inhibition has been reported to be associated with side effects.[6,7] PDE catalytic domains all share a hydrophobic clamp that binds the "purine"-like core of the cyclic nucleotides and form key hydrogen bonds to the common glutamine. For the dual substrate PDEs, this residue can rotate to form donor−acceptor hydrogen bonds to both cGMP and cAMP.[8]

The widespread distribution of PDEs in the central nervous system (CNS) and critical role of GPCR signaling in neurotransmission prompted the development of a PDE family initiative to identify potential therapeutic utility for centrally penetrant PDE inhibitors.[9] We have previously reported the discovery of multiple series of PDE10A inhibitors[10] including a

selective PDE10A inhibitor (PF-02545920) that has been administered to patients and completed a phase 2 trial in schizophrenia.[11] We have used the experience gained executing these programs to explore the development of selective brain penetrant PDE9A inhibitors.

It has been reported that cGMP elevation can cause an increase in synaptic transmission and long-term potentiation.[12] In addition it has been shown that cGMP can reverse $A\beta$ induced deficits in long-term potentiation in hippocampal slices.[13] PDE9A is a cGMP specific phosphodiesterase with the highest affinity of all PDEs for cGMP with $K_m = 170$ nM.[14] The exquisite potency for cGMP hydrolysis combined with the widespread distribution[15] of PDE9A makes it an excellent target for globally elevating cGMP to test this hypothesis in the treatment of cognitive disruption in diseases such as Alzheimer's disease.[16]

■ RESULTS AND DISCUSSION

We have previously described the utilization of parallel medicinal chemistry to enable the potential synthesis of thousands of pyrazolopyrimidines exemplified by HTS hit **1**. Utilizing prospective physicochemical property based design coupled with the targeting of key residue differences within the PDEs and in particular the residue differences between PDE1C and PDE9A, we developed a brain penetrant in vivo tool **2** (PF-04181366) that can elevate cGMP in brain tissue (Figure 1).[17]
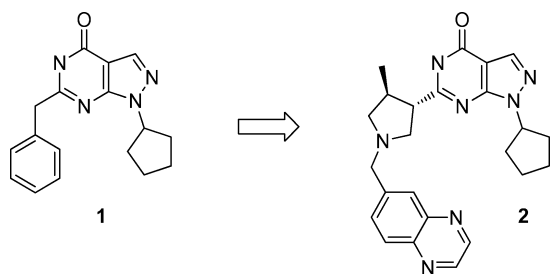
Figure 1. Development of in vivo active lead **2**.

Although compound **2** had high potency against PDE9A (1.8 nM) and selectivity over PDE1C (50-fold), it possessed high human liver microsomal clearance (149 mL/min/kg) resulting in a projected large dose and a short half-life.[18] High selectivity had been achieved with **2** over all the PDEs except PDE1C. PDE1C is expressed in cardiac tissue, so further selectivity was desired to advance a molecule into clinical trials. Therefore, our goal was to move beyond the development of a centrally penetrant tool to identify a more selective PDE9A inhibitor with improvements in pharmacokinetics and safety that could be taken into clinical trials. Our strategy to improve the pharmacokinetics of our lead molecule **2** again utilized parallel chemistry to target rapid replacement of the lipophilic cyclopentyl group with more polar functionality. On the basis of the X-ray crystal structure of **1**, which has been previously cocrystallized in the PDE9A catalytic domain (Figure 2), we hypothesized that an increase in polarity would also improve our selectivity over PDE1C, since PDE9A has a more polar inhibitor binding environment with the presence of tyrosine-424 versus a corresponding phenyl alanine-441 in PDE1C.

In addition, this strategy to design molecules with reduced lipophilicity should improve the P450-mediated clearance of the targeted compounds. The replacement of the cyclopentyl group in compound **1** was explored by building the pyrazole
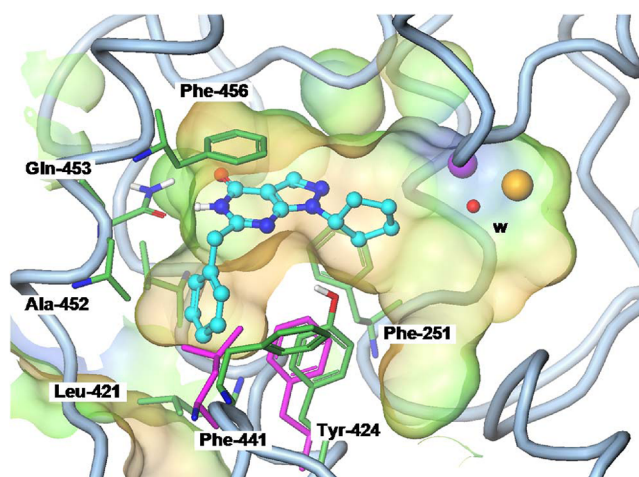
Figure 2. PDE9A inhibitor **1** (PDB code 3JSI) bound and structural differences with PDE1C (pink).

ring from a variety of commercial and custom hydrazines. This effort identified a 4-tetrahydropyran derivative **3**, which significantly improved the human liver microsomal clearance from 200 to 14 mL/min/kg without impacting the P-glycoprotein (P-gp) efflux ratio (Table 1). Additionally this came with an improvement in lipophilic binding efficiency (LipE)[19] from 6.75 to 8.5. These characteristics aligned the in vitro ADME properties and binding efficiencies with what is reported for CNS marketed drugs.[20] By increase of the polarity, a 14-fold improvement in selectivity over PDE1c was established and validated our design strategy. On the basis of the cocrystal structures, the improvement in selectivity appeared to be driven by the pyran oxygen interacting through a water hydrogen bonding network to tyrosine residue 424 in PDE9A, which in PDE1C is a phenylalanine. The loss in potency for PDE1C can be rationalized as being due to an increase in the desolvation penalty to accommodate the more polar tetrahydopyran into the more lipophilic environment in PDE1C formed by the Tyr to Phe mutations (Figure 2).

Incorporating the tetrahydropyran group with the benzyl-pyrrolidine motif in compound **2** was paramount to identifying compounds with further improvements in PDE1C selectivity. Condensing 4-hydrazinetetrahydropyran with the 2-(ethoxymethylene)malononitrile with base provided the cyanopyrazole (Scheme 1). Oxidation of the cyano to the carboxamide was achieved with aqueous hydrogen peroxide. Pyrrolidine esters were then coupled with the pyrazoloaminoamide to provide the benzyl analogues. The benzylpyrrolidine is an enabled monomer that can rapidly be deprotected and functionalized via reductive amination or alkylation to afford the fully functionalized products.

As we had hypothesized, the combination of the pyran and the pyrolidine moiety afforded a highly potent 4.9 nM and selective PDE9 inhibitor with improved pharmacokinetic properties. Significant improvements from compound **2** included increased selectivity (>200× over PDE1C) and a 5-fold reduction in clearance measured by human liver microsomes. It was determined that most of the activity resided in the enantiomer exemplified by compound **8**, which was 30-fold more potent than the less active enantiomer **9**.

Structure-based design identified an opportunity to improve potency by completely filling the pocket that the methyl on pyrrolidine compound **8** accessed. Modeling of an ethyl group

Table 1[a]
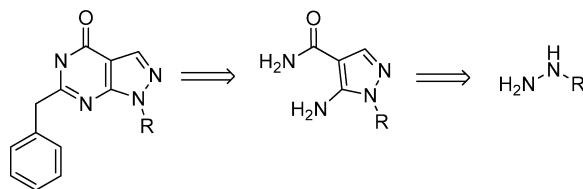
	R=	PDE9A	PDE1C	HLM	MDR BA/AB	ClogP	LipE
1	(cyclopentyl)	0.8 nM	0.4 nM	200	1.3	2.34	6.75
3	(tetrahydropyran)	1.0 nM	14 nM	14	1.3	0.50	8.5

[a]PDE9A and PDE1C: potency reported in nM as average of $n = 4$. HLM human liver microsomal clearance is in mL/min/kg. MDR is the efflux ratio BA/AB. LipE= $-\log K_i - $ ClogP.
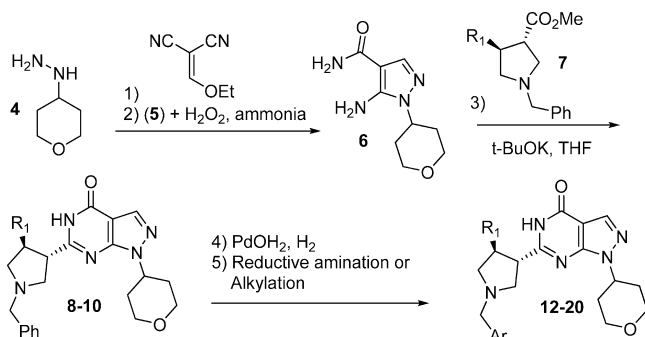
Scheme 1[a]

[a](a) Step 1: 2-(ethoxymethylene)malononitrile (1 equiv), triethylamine (4 equiv), ethanol (0.3 M), reflux 2 h. Step 2: 35% aq H_2O_2, aq ammonia, ethanol, 48 h. Step 3: pyrolidine ester (2 equiv), THF (0.1 M), 1.0 M *t*-BuOK (in THF, 2 equiv), reflux 16 h. Step 4: PdOH$_2$ (10%), conc HCl (1 equiv), methanol, 40 psi of H$_2$ 18 h. Step 5: reductive amination, aldehyde, 1,2-dichloroethane, sodium triacetoxyborohydride, 50 °C, 18 h; or alkylation, 2-(chloromethyl)-pyrimidine−HCl, cesium carbonate, iron triflate, DMF, 60 °C, 24 h.

Figure 3. The methyl group on the pyrrolidine does not completely fill the lipophilic pocket of PDE9A (circled area) (PDB code 3JSW).

analogue into the crystal structure was projected to optimize the space filling of the lipophilic pocket in PDE9A (see Figure 3).

Addition of an ethyl group in compound **10** did enhance potency (3-fold) but did not show an improvement in LipE or selectivity and displayed a higher human liver microsomal clearance (Table 2), rendering this avenue less appealing. Removal of the benzyl moiety in **11** afforded a compound that had low human liver microsomal clearance but with a significant loss in potency.[21]

While compound **8** displayed many desirable attributes to advance as a candidate molecule into clinical trials, the human liver microsomal clearance was still moderate. Compound **8** has a significant plasma protein binding free fraction of 40% due to the polarity of the molecule ClogP = 0.97. While plasma protein binding does not impact the dose, high free fractions can lead to a decreased half-life projection in humans, since a large amount of free drug is available to metabolize.[22] To ensure that a clinical compound from this series with low
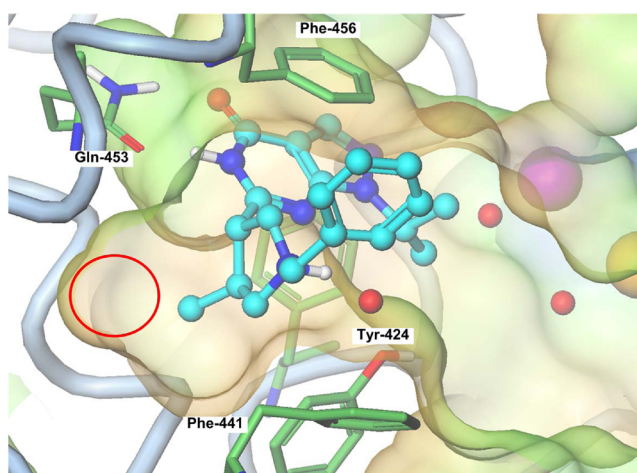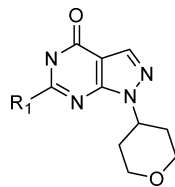
plasma protein binding and a moderate volume of distribution could be dosed once or twice a day, it was necessary to have a compound with very low human liver microsomal clearance to achieve an acceptable half-life in humans. Lowering the clearance of the molecule would also have a positive impact on the dose projection in humans. The enabled pyrrolidine monomer rapidly allowed for SAR generation to identify either substituents on the phenyl ring or incorporation of heterocycles to drive down P450-mediated clearance.

Fluorination of the phenyl ring did not reduce the clearance of the molecules, and only the para-fluoro substituent had equivalent clearance to the unsubstituted phenyl ring. This suggested that utilizing a blocking strategy with a fluorine to deactivate the phenyl ring to reduce P450-mediated oxidation was not likely to improve the dose or half-life projection. The increased clearance in these fluorinated analogues is probably driven through the increase in lipophilicity. Alternatively, lowering lipophilicity by incorporation of a heteroatom into the phenyl ring proved to be fruitful on multiple fronts. As expected, human liver microsomal clearance tracked with the lipophilicity of the compounds. Incorporation of one

Table 2[a]

	R1=	PDE9A	PDE1C	HLM	MDR BA/AB	ClogP	LipE
8	Me—(pyrrolidine)—N—Ph	4.9 nM	>1000 nM	39.5	1.5	0.97	7.34
9	Me—(pyrrolidine)—N—Ph	152 nM	5601 nM	17.0	1.53	0.97	5.85
10	Et—(pyrrolidine)—N—Ph	1.7 nM	431 nM	89.8	1.42	1.50	7.26
11	Me—(pyrrolidine)—N—H	89 nM	3421 nM	<7.1	NA	-1.26	8.31

[a]PDE9A and PDE1C: potency reported in nM as average of $n = 4$. HLM human liver microsomal clearance is in mL/min/kg. MDR is the efflux ratio BA/AB. LipE= $-\log K_i - $ ClogP. NA = unable to measure flux in MDR potentially because of poor permeability.

heteroatom into the ring decreased the microsomal clearance by half for compounds **16** and **17**. Subsequently, pyrimidines and pyrazines were incorporated to determine if the clearance could be lowered further with addition of another heteroatom and concomitant lowering of the lipophilicity. It was determined that the pyrimidine compounds **19** and **20** could effectively render the compounds completely stable to P450-mediated oxidation in the in vitro human liver microsomal system.

While these heteroaryl compounds were highly polar with negative ClogP values, compounds within this series still maintained brain penetration. Interesting trends were seen with the P-gp MDR efflux ratios, which are predictive of brain penetration in humans. CNS compounds that exhibit no central penetration impairment typically have an efflux ratio of <2.5. The 2-pyridyl substitution **16** provided significantly less P-gp efflux liability than the 3-substituted pyridine **17** (1.44 vs 4.49) (Table 3). To further explore this trend, the 2,6-pyrimidine was compared to the 3,5-pyrimidine, and this effect was even more pronounced. The 2,6-pyrimidine 6-[(3S,4S)-4-methyl-1-(pyrimidin-2-ylmethyl)pyrrolidin-3-yl]-1-(tetrahydro-2H-pyran-4-yl)-1,5-dihydro-4H-pyrazolo[3,4-d]pyrimidin-4-one (PF-04447943)[30] **20** with a ClogP of −1.5 displayed an MDR ratio of 1.23, while the 3,5-pyrimidine showed an efflux ratio of 15.8. This ratio proved highly predictive in that compound **20** displayed good brain penetration in the rat and compound **19** showed a very low brain to plasma ratio (<0.05). The differential brain penetration and P-gp efflux liability cannot be explained by traditional physicochemical properties, since

the differences in molecular weight, basic pK_a, lipophilicity, and polar surface area are negligible. Future publications will explore the cause and generality of these findings.

Alignment of the desired in vitro ADME properties was achieved with compound **20**, and just as importantly potency for PDE9A inhibition was maintained as lipophilicity was decreased. This is demonstrated with the heterocyclic compounds exhibiting improved LipE over the phenyl compounds. The LipE was further improved via incorporation of the pyrimidines, culminating in compound **20** with a LipE of 9.58. LipE for **20** is exquisitely high when compared to typical enzyme inhibitors and marketed CNS drugs.

The X-ray structure of **20** cocrystallized in the catalytic domain of PDE9A (Figure 4) shows that unique features of interaction with PDE9A. While the traditional interactions with Gln-453 are maintained, the pyrimidine ring is stacking with the Phe-441. It appears that this stacking is not driven by lipophilicity in that the heterocyclic analogues are essentially equipotent to the phenyl ring. An edge on interaction with Phe-456 is also observed. The water molecule mediating the ligand Tyr-424 interaction is also observed and could potentially donate a hydrogen bond to the nitrogen of the pyrimidine ring of **20** at a distance of 2.9 Å. Compound **20** possessed all of the desired in vitro attributes that were targeted to advance into candidate selection including potency (8 nM), selectivity (>10 μM versus all the PDEs except PDE1C at >1 μM), low human liver microsomal clearance (<8), and no P-gp liability. Evaluation of **20** in the CEREP panel screen showed less than 50% activity against a 75+ panel of GPCRs, enzymes, and

Table 3[a]
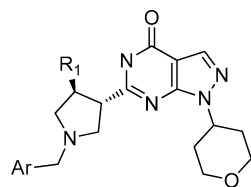
	R1=	AR	PDE9A	PDE1C	HLM	MDR BA/AB	ClogP	LipE
12	Me		4.6 nM	889 nM	127	1.51	1.12	7.21
13	Me		1.2 nM	693 nM	114	1.33	1.12	7.80
14	Me		0.9 nM	165 nM	60	1.50	1.12	7.92
15	Me		3.4 nM	466 nM	17		0.89	7.56
16	Me		6.3 nM	1858 nM	15	1.75	-0.52	8.72
17	Me		3.8 nM	979 nM	19	4.49	-0.02	8.44
18	Me		12 nM	1603 nM	9	2.99	-0.98	8.90
19	Me		4.6 nM	1872 nM	<8	15.8	-0.98	9.31
20	Me		8.3 nM	1394 nM	<8	1.23	-1.5	9.58

[a]PDE9A and PDE1C: potency reported in nM as average of $n = 4$. HLM human liver microsomal clearance is in mL/min/kg. MDR is the efflux ratio BA/AB. LipE= $-\log K_i - $ ClogP.

ion channels when tested at 10 μM. This selectivity was achieved by optimizing the physicochemical properties of the molecule and by interacting with two unique residues in PDE9A vs PDE1C. As was designed, polar interactions with tyrosine-424 in PDE9A (vs phenylalanine in PDE1C) by the pyrrolidine and incorporation of a more polar pyran provided significant selectivity. Additionally selectivity was gained via a π-stacking interaction between the 2,6-pyrimidine and phenylalanine 441 in PDE9A, which is an isoleucine in PDE1C.

Compound **20** was centrally penetrant in rodents as evidenced by brain to plasma ratios ranging from 0.59 to 0.88 in rats and mice, respectively. There was a slight disequilibrium in free drug concentrations across the central compartment, as evidenced by free brain/free plasma ratios
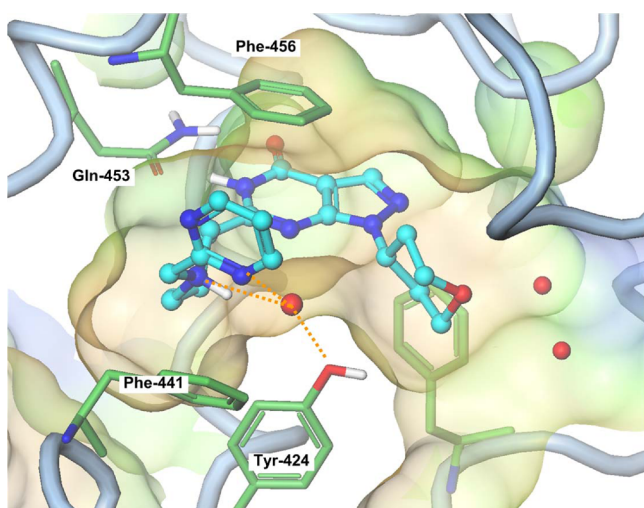
Figure 4. X-ray crystal structure of PDE9A inhibitor **20** (PDB code 4E90) bound in PDE9A making key interaction with the phenylalanine and tyrosine to provide selectivity over PDE1C.

ranging from 0.32 to 0.52 (rats and mice, respectively) and by a cerebrospinal fluid (CSF)/free plasma equal to 0.19 (rat). These findings indicate some impairment in the compound's ability to cross the rodent blood−brain barrier. The disequilibrium in free drug concentrations was further evaluated to determine species specificity and potential human translation and was predicted to be a rodent-specific finding mediated by efflux via P-gp (cross-species in vitro transporter evaluation). Additional experiments examining CSF and plasma concentration−time profiles in the dog resulted in no evidence of disequilibrium ($AUC_{csf}/AUC_{p,u}$ equal to 0.93) in this higher species.

The pharmacokinetic properties of compound **20** were determined in both the rat and dog. The in vivo clearance of compound **20** was moderate in the rat and low in the dog, in agreement with in vitro clearance estimates generated using liver microsomes (Table 4). The volume of distribution was

Table 4. Summary of Preclinical Pharmacokinetic Parameters of Compound 20[a]

	rat	dog	human
microsomal CL_b[b] (mL/min/kg)	<22.1	<17.4	<5.3
in vivo CL_b (mL/min/kg)	32.1	11.7	NA
ivivc	1.5×	1.5×	NA

[a]CL_b determined from rat and dog following iv administration at 1 and 0.3 mg/kg, respectively. NA = not applicable. ivivc = in vitro to in vivo correlation. [b]Calculated using the well-stirred model with the inclusion of all binding factors.

determined to be moderate across species (∼2 L/kg), and the bioavailability ranged from 73% to 91% in rats and dogs, respectively. In humans, compound **20** was projected to have a low systemic clearance through the use of preclinical/in vitro clearance prediction methodology.[23] Additional information on the preclinical and clinical pharmacokinetics and exposure−response relationships will be reported in a future publication.

With desirable potency, selectivity, and pharmacokinetic properties, compound **20** has been the subject of extensive biological profiling using models of CNS function and dysfunction. It has been shown to elevate cGMP in multiple brain regions and in cerebral spinal fluid (CSF), which provided

the opportunity for a translatable biomarker to assess target engagement. Electrophysiological evaluation of compound **20** under select conditions has revealed an impact on hippocampal synaptic plasticity, as represented by long-term potentiation. In vivo studies demonstrate that auditory gating deficits produced by amphetamine can be reversed in a dose-dependent fashion with **20**, suggesting the potential for utility in a variety of human disease states that exhibit a disrupted P50-gating response including schizophrenia, Huntington's disease, and Alzheimer's disease.[24] Procognitive activity in a variety of rodent models has been demonstrated by multiple groups. Compound **20** was efficacious in both a spatial recognition memory model and a novel object recognition model, which both rely on time-dependent disruption of episodic memory.[25] In addition, compound **20** was able to reverse scopolamine-induced deficits in both the Morris water maze and novel object recognition, suggesting potential therapeutic utility in patients with slight impairments of the cholinergic system, such as mild cognitive impairment or early Alzheimer's disease. Evidence that **20** can reverse deficits produced by the NMDA receptor antagonist ketamine, at doses expected to produce moderate inhibition of the PDE9A enzyme, in a spatial memory task using an eight-arm radial maze suggests the potential for remediation of cognitive deficits across a variety of disease states exhibiting impaired glutamate neurotransmission.[26] Finally, preliminary evidence of synaptic stabilization in the Tg2576 mouse model of amyloid precursor protein (APP) overexpression is suggested by data showing that chronic exposure to **20** prevented the loss in hippocampal dendritic spine density that normally occurs in this transgenic model between 4 and 5 months of age.[27] Efficacy in this potential synaptoprotective model occurred with chronic exposures equivalent to efficacy seen in the cognition models and correlated with a CSF cGMP elevation of ∼125−150%

■ CONCLUSION

Through parallel chemistry and structure-based design, clinical candidate **20** was identified to answer biological questions for a centrally penetrant PDE9A inhibitor in humans. In particular, PDE9A inhibition may improve cognition in multiple disease states. Compound **20** shows excellent selectivity within the PDE family and in broad ligand profiling. The physicochemical properties of the molecule show that a highly polar molecule (ClogP < 0) can still have CNS penetration if other physicochemical properties are balanced such as limiting the number of hydrogen bond donors, lowering the basic pK_a, and minimizing the molecular weight.[28] The broad efficacy in multiple preclinical cognition models including the potential for synaptic stabilization in the Tg2576 mouse model has supported the advancement of **20** into clinical trials. The promising preclinical pharmacokinetic properties has translated to phase 1 clinical trials. In humans, **20** has excellent tolerability, exposure, and a half-life of 19−31 h.[29] The preclinical CSF elevation of cGMP has translated to humans, and it has been reported that a single dose of 40 mg elevated CSF cGMP by ∼300%.[30] The translation of the central preclinical cGMP response to humans is proof that **20** is a viable clinical compound to test in multiple clinical populations that display cognitive deficits.

■ EXPERIMENTAL SECTION

All reagents and solvents were used as purchased from commercial sources. Reactions were carried out under a blanket of nitrogen. Silica

gel chromatography was done using the appropriate size Biotage prepacked silica filled cartridges. Mass spectral data were collected on a Micromass ADM atmospheric pressure chemical ionization instrument (LRMS APCI). NMR spectra were generated on a Varian 400 MHz instrument. Chemical shifts were recorded in ppm relative to tetramethylsilane (TMS) with multiplicities given as s (singlet), bs (broad singlet), d (doublet), t (triplet), dt (doublet of triplets), m (multiplet). Compound purity is determined by combustion analysis (Quantitative Technologies, Inc.) or high pressure liquid chromatography (HPLC). The purity of title compounds used in pharmacology testing was verified by HPLC–MS using the following method: 12 min gradient on a HP1100C pump of increasing concentrations of acetonitrile in water (5% → 95%) containing 0.1% formic acid with a flow rate of 1 mL/min and UV detection at λ 220 and 254 nm on a Gemini C18 150 mm × 4.6 mm, 5 μm column (Phenomenex, Torrance, CA). All final compounds either met combustion analysis within ±0.4% or were >95% pure by HPLC by one of the methods above.

6-Benzyl-1-(tetrahydro-2*H*-pyran-4-yl)-1*H*-pyrazole[3,4-*d*]-pyrimidin-4(5*H*)-one (3). To a solution of 5-amino-1-(tetrahydro-2*H*-pyran-4-yl)-1*H*-pyrazole-4-carboxamide **6** (100 mg, 0.476 mmol) in 4.8 mL of absolute ethanol was added ethyl 2-phenylacetate (352 mg, 2.14 mmol, 4.5 equiv) and then NaH (99 mg, 2.48 mmol, 5.2 equiv). The resulting heterogeneous mixture was heated in a microwave at 150 °C for 30 min. After cooling to ambient temperature, the resulting mixture was concentrated. The crude material was purified with a 0–10% NH$_4$OH in methanol/ethyl acetate gradient to afford the desired material (130 mg, 88% yield) as a white solid. 400 MHz ^{1}H NMR (CDCl$_3$) δ 11.32 (s, 1H), 8.10 (s, 1H), 7.46–7.29 (m, 5H), 4.92 (m, 1H), 4.19 (dd, J = 11.5, 3.8 Hz, 2H), 4.11 (s, 2H), 3.67 (t, J = 11.4 Hz, 2H), 2.49–2.38 (m, 2H), 2.00–1.96 (m, 2H). MS: M$^+$H m/z = 311.3.

1-(Tetrahydro-2*H*-pyran-4-yl)hydrazine (4). To a solution of tetrahydropyran-4-one (71.6 g, 715 mmol) in methanol (2 L) was added *tert*-butylcarbazate (100 g, 758 mmol) at ambient temperature. The mixture was stirred at ambient temperature for 20 h. The reaction mixture was concentrated under reduced pressure to dryness to afford a white solid (154 g). To a suspension of the white solid (154 g, 715 mmol) in water (1 L) was added acetic acid (500 mL, 8.73 mol), and the mixture was stirred for 30 min to get a clear solution. To this solution, solid NaCNBH$_3$ (44.5 g, 708 mmol) was added portionwise. The mixture was stirred at ambient temperature for 2 h. The mixture was then transferred to a 12 L flask, cooled to 0 °C, and quenched with 1 N NaOH (8.73 L, 8.73 mol). The mixture was extracted with CH$_2$Cl$_2$ (3 × 3 L) and dried over Na$_2$SO$_4$. The organic layer was filtered and concentrated to afford a white solid (164 g, contains ~15% of *N*-acetyl-*N*′-Boc-hydrazine derivative). Chromatography [silica, ethyl acetate/MeOH (95:5)] gave 94 g of 90% pure Boc-hydrazine. A solution of Boc-hydrazine (50 g, 231 mmol) in methanol (500 mL) was added to a solution of HCl in dioxane (462 mL, 1.85 mol, 4.0 M). The mixture was stirred at ambient temperature overnight. Concentration of the reaction mixture under reduced pressure afforded the title compound as a white solid (43 g, 98%). 400 MHz ^{1}H NMR (DMSO) δ 3.85–3.82 (m, 2H), 3.27–3.21 (m, 2H), 3.13–3.05 (m, 1H), 1.88–1.84 (m, 2H), 1.48–1.38 (m, 2H). MS: M + H m/z = 117.2.

5-Amino-1-(tetrahydro-2*H*-pyran-4-yl)-1*H*-pyrazole-4-carbonitrile (5). To a mixture of 1-(tetrahydro-2*H*-pyran-4-yl)hydrazine dihydrogen chloride **4** (18 g, 96 mmol) in 200 mL of ethanol was added triethylamine (30 g, 40 mL, 288 mmol) at 0 °C (ice bath). The resulting mixture was stirred for 1 h. Then a solution of 2-(ethoxymethylene)malononitrile (12 g, 96 mmol) in 100 mL of ethanol was added slowly to keep the reaction temperature below 5 °C. This mixture was stirred at ambient temperature overnight and then heated to reflux for 2 h. After removal of the solvent under vacuum, the residue was washed with 300 mL of water. The solid was collected, washed with additional 200 mL of water and 200 mL of 1:1 of hexane and ether, and dried to give 17 g of yellow solid. 400 MHz ^{1}H NMR (CD$_3$OD) δ 7.71 (s, 1H), 4.29–4.21 (m, 1H), 4.02 (dd, J = 11.6, 4.6 Hz, 2H), 3.28 (t, J = 1.7 Hz, 2H), 2.12–2.02 (m, 2H), 1.80–1.76 (m, 2H). MS: M$^+$H m/z = 193.1.

5-Amino-1-(tetrahydro-2*H*-pyran-4-yl)-1*H*-pyrazole-4-carboxamide (6). A stirred solution of 5-amino-1-(tetrahydro-2*H*-pyran-4-yl)-1*H*-pyrazole-4-carbonitrile **5** (228 mmol) in ethanol (300 mL) was treated with 35% aqueous H$_2$O$_2$ (100 mL) followed by aqueous ammonia (300 mL). The reaction mixture was stirred for 48 h at ambient temperature and then quenched with saturated sodium thiosulfate (800 mL) and concentrated under reduced pressure to remove most of the ethanol. The resulting solid was removed by filtration and washed with water (2 × 200 mL) and ether (2 × 150 mL). The solid was dried in vacuo to constant weight (31 g, 65% yield for two steps). 400 MHz ^{1}H NMR (CD$_3$OD) δ 7.67 (s, 1H), 4.27–4.21 (m, 1H), 4.03 (dd, J = 11.6, 4.6 Hz, 2H), 3.28 (t, J = 1.7 Hz, 2H), 2.14–2.04 (m, 2H), 1.81–1.78 (m, 2H). MS: M$^+$H m/z = 211.2.

6-[(3*S*,4*S*)-1-Benzyl-4-methylpyrrolidin-3-yl]-1-(tetrahydro-2*H*-pyran-4-yl)-1,5-dihydro-4*H*-pyrazolo[3,4-*d*]pyrimidin-4-one (8). To a mixture of 5-amino-1-(tetrahydro-2*H*-pyran-4-yl)-1*H*-pyrazole-4-carboxamide (5.0 g, 23.78 mmol) and (3,4-*trans*)-methyl 1-benzyl-4-methylpyrrolidine-3-carboxylate (11.7 g, 47.57 mmol) in tetrahydrofuran (0.1 M) were added molecular sieves (pellets). To the stirred mixture was added a 1.0 M solution of *t*-BuOK in THF (48.0 mL, 47.57 mmol), and the resulting mixture was heated at reflux under an atmosphere of nitrogen with vigorous stirring overnight. The reaction mixture was cooled to ambient temperature, and solids were removed by filtration. The solids were washed with EtOAc (2×), and the combined filtrates were concentrated under reduced pressure. The remainder was partitioned between CH$_2$Cl$_2$ and H$_2$O, and the aqueous and organic layers were separated. The aqueous phase was extracted with CH$_2$Cl$_2$ (1×), and the combined organic extracts were dried over Na$_2$SO$_4$, filtered, and concentrated under reduced pressure. The crude material was purified by chromatography (silica gel, 1% Et$_3$N in EtOAc) to produce (6.6 g, 68% yield) as a white solid. The enantiomers were separated utilizing chiral chromatography with Chiralcel OD-H, mobile phase 70/30 heptane/EtOH, t_R = 11.465 (more active enantiomer **3**), to provide the two enantiomers in >98% ee. 400 MHz ^{1}H NMR (CDCl$_3$) δ 8.02 (s, 1H), 7.39–7.25 (m, 6H), 4.83–4.75 (m, 1H), 4.14–4.09 (m, 2H), 3.82 (m, 1H), 3.62–3.54 (m, 3H), 3.39–3.37 (m, 1H), 3.00 (m, 1H), 2.83 (m, 1H), 2.66–2.27 (m, 4H), 2.10–1.83 (m, 3H), 1.20 (d, J = 6.6 Hz, 3H). MS: M$^+$H m/z = 394.2.

6-[(3*R*,4*R*)-1-Benzyl-4-methylpyrrolidin-3-yl]-1-(tetrahydro-2*H*-pyran-4-yl)-1,5-dihydro-4*H*-pyrazolo[3,4-*d*]pyrimidin-4-one (9). 400 MHz ^{1}H NMR (CDCl$_3$) δ 8.02 (s, 1H), 7.39–7.25 (m, 6H), 4.82–4.76 (m, 1H), 4.14–4.09 (m, 2H), 3.82–3.79 (m, 1H), 3.62–3.54 (m, 3H), 3.37 (d, J = 8.7 Hz, 1H), 3.00 (d, J = 9.9 Hz, 1H), 2.79 (dd, J = 6.3, 2.5 Hz, 1H), 2.52–2.48 (m, 1H), 2.42–2.30 (m, 3H), 1.94–1.82 (m, 3H), 1.20 (d, J = 6.6 Hz, 3H). MS: M$^+$H m/z = 394.2.

6-[(3,4-*trans*)-1-Benzyl-4-ethylpyrrolidin-3-yl]-1-(tetrahydro-2*H*-pyran-4-yl)-1,5-dihydro-4*H*-pyrazolo[3,4-*d*]pyrimidin-4-one (10). Following the procedure for the preparation of 6-[(3*S*,4*S*)-1-benzyl-4-methylpyrrolidin-3-yl]-1-(tetrahydro-2*H*-pyran-4-yl)-15-dihydro-4*H*-pyrazolo[3,4-*d*]pyrimidin-4-one (**8**) but substituting *trans*-methyl 1-benzyl-4-ethylpyrrolidine-3-carboxylate provided the title compound. Preparative conditions: Chiralcel OJ-H, mobile phase 80/20 CO$_2$/MeOH, t_R = 3.27. Analytical: AD column, mobile phase 85/15 heptane/EtOH, t_R = 12.896. 400 MHz ^{1}H NMR (CDCl$_3$) δ 8.02 (s, 1H), 7.40–7.26 (m, 5H), 4.78 (m, 1H), 4.12–4.09 (m, 2H), 3.82–3.804 (m, 1H), 3.65–3.54 (m, 3H), 3.35 (t, J = 8.3 Hz, 1H), 2.98 (d, J = 9.9 Hz, 1H), 2.89–2.86 (m, 1H), 2.48–2.32 (m, 3H), 2.20 (m, 1H), 1.95–1.87 (m, 2H), 1.63–1.58 (m, 2H), 1.50–1.49 (m, 1H), 0.93 (t, J = 7.1 Hz, 3H). MS: M + H m/z = 408.1.

6-[(3*S*,4*S*)-4-Methylpyrrolidin-3-yl]-1-(tetrahydro-2*H*-pyran-4-yl)-1*H*-pyrazolo[3,4-*d*]pyrimidin-4(5*H*)-one (11). 6-[(3*S*,4*S*)-1-Benzyl-4-methylpyrrolidin-3-yl]-1-(tetrahydro-2*H*-pyran-4-yl)-15-dihydro-4*H*-pyrazolo[3,4-*d*]pyrimidin-4-one (5.6 g) was dissolved in 100 mL of methanol, and the mixture was added to a Parr bottle. Palladium hydroxide (3.76 g) was added along with 3.56 mL of concentrated hydrochloric acid. The reaction mixture was placed on a hydrogenator under 40 psi of H$_2$ for 18 h. The reaction mixture was filtered through

Celite and concentrated to provide 4.47 g of the title compound as the hydrogen chloride salt. 400 MHz ^{1}H NMR (CD$_3$OD) δ 8.03 (s, 1H), 4.49 (m, 1H), 4.09–4.06 (m, 2H), 3.74–3.57 (m, 4H), 3.24 (m, 1H), 3.05 (m, 1H), 2.89 (m, 1H), 2.77 (m, 1H), 2.30 (m, 2H), 1.90 (m, 2H), 1.22 (d, J = 6.6 Hz, 3H). MS: M$^+$H m/z = 304.2.

6-[(3S,4S)-1-(2-Fluorobenzyl)-4-methylpyrrolidin-3-yl]-1-(tetrahydro-2H-pyran-4-yl)-1,5-dihydro-4H-pyrazolo[3,4-d]-pyrimidin-4-one (12). Following the procedure for the preparation of 6-{(3S,4S)-4-methyl-1-[(2-methylpyrimidin-5-yl)methyl]pyrrolidin-3-yl}-1-(tetrahydro-2H-pyran-4-yl)-15-dihydro-4H-pyrazolo[3,4-d]-pyrimidin-4-one (19) but substituting 2-fluorobenzaldehyde provided the title compound. 400 MHz ^{1}H NMR (CD$_3$OD) δ 7.98 (s, 1H), 7.47–7.42 (m, 1H), 7.33–7.26 (m, 2H), 7.18–7.07 (m, 1H), 4.08–4.04 (m, 2H), 3.85 (s, 2H), 3.69–3.56 (m, 3H), 3.20–2.93 (m, 4H), 2.69–2.62 (m, 1H), 2.40–2.19 (m, 3H), 1.88–1.85 (m, 2H), 1.14 (d, J = 6.6 Hz, 3H). MS: M + H m/z = 412.1.

6-[(3S,4S)-1-(3-Fluorobenzyl)-4-methylpyrrolidin-3-yl]-1-(tetrahydro-2H-pyran-4-yl)-1,5-dihydro-4H-pyrazolo[3,4-d]-pyrimidin-4-one (13). Following the procedure for the preparation of 6-{(3S,4S)-4-methyl-1-[(2-methylpyrimidin-5-yl)methyl]pyrrolidin-3-yl}-1-(tetrahydro-2H-pyran-4-yl)-15-dihydro-4H-pyrazolo[3,4-d]-pyrimidin-4-one (19) but substituting 3-fluorobenzaldehyde provided the title compound. 400 MHz ^{1}H NMR (CDCl$_3$) δ 8.02 (s, 1H), 7.35–7.30 (m, 1H), 7.21–7.20 (m, 1H), 7.05 (d, J = 9.5 Hz, 1H), 6.98–6.93 (m, 1H), 4.83–4.77 (m, 1H), 4.14–4.08 (m, 2H), 3.80–3.77 (m, 1H), 3.64–3.54 (m, 3H), 3.36 (t, J = 8.8 Hz, 1H), 3.01 (d, J = 9.9 Hz, 1H), 2.84–2.83 (m, 1H), 2.57 (m, 1H), 2.44–2.27 (m, 3H), 1.95–1.83 (m, 3H), 1.20 (d, J = 7.1 Hz, 3H). MS: M + H m/z = 412.4.

6-[(3S,4S)-1-(4-Fluorobenzyl)-4-methylpyrrolidin-3-yl]-1-(tetrahydro-2H-pyran-4-yl)-1,5-dihydro-4H-pyrazolo[3,4-d]-pyrimidin-4-one (14). Following the procedure for the preparation of 6-{(3S,4S)-4-methyl-1-[(2-methylpyrimidin-5-yl)methyl]pyrrolidin-3-yl}-1-(tetrahydro-2H-pyran-4-yl)-15-dihydro-4H-pyrazolo[3,4-d]-pyrimidin-4-one 19 but substituting 4-fluorobenzaldehyde provided the title compound. 400 MHz ^{1}H NMR (CDCl$_3$) δ 8.02 (s, 1H), 7.36–7.33 (m, 2H), 7.05–7.01 (m, 2H), 4.82–4.77 (m, 1H), 4.14–4.09 (m, 2H), 3.79–3.76 (m, 1H), 3.62–3.54 (m, 3H), 3.34 (t, J = 8.3 Hz, 1H), 2.99 (d, J = 9.9 Hz, 1H), 2.85–2.83 (m, 1H), 2.60–2.55 (m, 1H), 2.45–2.30 (m, 3H), 1.99–1.82 (m, 3H), 1.20 (d, J = 7.1 Hz, 3H). MS: M + H m/z = 412.1.

6-[(3S,4S)-1-(4-Methoxybenzyl)-4-methylpyrrolidin-3-yl]-1-(tetrahydro-2H-pyran-4-yl)-1,5-dihydro-4H-pyrazolo[3,4-d]-pyrimidin-4-one (15). Following the procedure for the preparation of 6-{(3S,4S)-4-methyl-1-[(2-methylpyrimidin-5-yl)methyl]pyrrolidin-3-yl}-1-(tetrahydro-2H-pyran-4-yl)-15-dihydro-4H-pyrazolo[3,4-d]-pyrimidin-4-one 19 but substituting 4-methoxybenzaldehyde provided the title compound. 400 MHz ^{1}H NMR (CDCl$_3$) δ 8.01 (s, 1H), 7.29 (d, J = 8.3 Hz, 2H), 6.87 (d, J = 8.7 Hz, 2H), 4.82–4.08 (m, 1H), 4.13–4.08 (m, 2H), 3.84–3.75 (m, 4H), 3.61–3.51 (m, 3H), 3.35 (t, J = 8.7 Hz, 1H), 2.97 (d, J = 9.9 Hz, 1H), 2.82–2.80 (m, 1H), 2.53–2.49 (m, 1H), 2.42–2.30 (m, 3H), 1.95–1.82 (m, 3H), 1.18 (d, J = 7.1 Hz, 3H). MS: M + H m/z = 424.5.

6-{(3S,4S)-4-Methyl-1-[(6-methylpyridin-3-yl)methyl]-pyrrolidin-3-yl}-1-(tetrahydro-2H-pyran-4-yl)-1,5-dihydro-4H-pyrazolo[3,4-d]pyrimidin-4-one (16). Following the procedure for the preparation of 6-{(3S,4S)-4-methyl-1-[(2-methylpyrimidin-5-yl)methyl]pyrrolidin-3-yl}-1-(tetrahydro-2H-pyran-4-yl)-15-dihydro-4H-pyrazolo[3,4-d]pyrimidin-4-one 19 but substituting 6-methylnicotinaldehyde provided the title compound. 400 MHz ^{1}H NMR (CD$_3$OD) δ 8.38 (d, J = 2.1 Hz, 1H), 7.99 (s, 1H), 7.77 (d, J = 2.07 Hz, 1H), 7.75 (d, J = 2.07 Hz, 1H), 4.94–4.83 (m, 1H), 4.09–4.05 (m, 2H), 3.78–3.57 (m, 4H), 3.31–3.28 (m, 1H), 3.11–3.06 (m, 1H), 3.01–2.91 (m, 2H), 2.72–2.65 (m, 1H), 2.50 (s, 3H), 2.33–2.23 (m, 3H), 1.90–1.86 (m, 2H), 1.14 (d, J = 7.1 Hz, 3H). MS: M + H m/z = 409.2.

6-{(3S,4S)-4-Methyl-1-[(6-methylpyridin-3-yl)methyl]-pyrrolidin-3-yl}-1-(tetrahydro-2H-pyran-4-yl)-1,5-dihydro-4H-pyrazolo[3,4-d]pyrimidin-4-one (17). Following the procedure for the preparation of 6-{(3S,4S)-4-methyl-1-[(2-methylpyrimidin-5-yl)-methyl]pyrrolidin-3-yl}-1-(tetrahydro-2H-pyran-4-yl)-15-dihydro-4H-pyrazolo[3,4-d]pyrimidin-4-one 19 but substituting 6-methylnicotinaldehyde provided the title compound. 400 MHz ^{1}H NMR (CD$_3$OD) δ

8.38 (d, J = 2.1 Hz, 1H), 7.99 (s, 1H), 7.77 (d, J = 2.07 Hz, 1H), 7.75 (d, J = 2.07 Hz, 1H), 4.94–4.83 (m, 1H), 4.09–4.05 (m, 2H), 3.78–3.57 (m, 4H), 3.31–3.28 (m, 1H), 3.11–3.06 (m, 1H), 3.01–2.91 (m, 2H), 2.72–2.65 (m, 1H), 2.50 (s, 3H), 2.33–2.23 (m, 3H), 1.90–1.86 (m, 2H), 1.14 (d, J = 7.1 Hz, 3H). MS: M + H m/z = 409.2.

6-{(3S,4S)-4-Methyl-1-[(5-methylpyrazin-2-yl)methyl]-pyrrolidin-3-yl}-1-(tetrahydro-2H-pyran-4-yl)-1,5-dihydro-4H-pyrazolo[3,4-d]pyrimidin-4-one (18). Following the procedure for the preparation of 6-{(3S,4S)-4-methyl-1-[(2-methylpyrimidin-5-yl)-methyl]pyrrolidin-3-yl}-1-(tetrahydro-2H-pyran-4-yl)-15-dihydro-4H-pyrazolo[3,4-d]pyrimidin-4-one 19 but substituting 5-methylpyrazine-2-carbaldehyde provided the title compound. 400 MHz ^{1}H NMR (CDCl$_3$) δ 8.53 (s, 1H), 8.47 (s, 1H), 8.03 (s, 1H), 4.83–4.79 (m, 1H), 4.12–4.03 (m, 2H), 3.78–3.75 (m, 1H), 3.61–3.55 (m, 2H), 3.46–3.40 (m, 1H), 3.12–3.09 (m, 1H), 2.87 (m, 1H), 2.64 (m, 1H), 2.53 (m, 2H), 2.47–2.28 (m, 4H), 2.16 (m, 2H), 1.91–1.84 (m, 2H), 1.23–1.20 (m, 3H). MS: M + H m/z = 410.3.

6-{(3S,4S)-4-Methyl-1-[(2-methylpyrimidin-5-yl)methyl]-pyrrolidin-3-yl}-1-(tetrahydro-2H-pyran-4-yl)-1,5-dihydro-4H-pyrazolo[3,4-d]pyrimidin-4-one (19). To a solution of 6-[(3S,4S)-4-methylpyrrolidin-3-yl]-1-(tetrahydro-2H-pyran-4-yl)-1H-pyrazolo-[3,4-d]pyrimidin-4(5H)-one hydrogen chloride (493 mg) in 1,2-dichloroethane (10 mL) were added acetic acid (174 mg), 2-methylpyrimidine-5-carbaldehyde (236 mg), and sodium triacetoxyborohydride (635 mg). The reaction mixture was heated at 50 °C overnight. The reaction mixture was concentrated onto silica gel and purified by CombiFlash chromatography to provide the title compound (146 mg). 400 MHz ^{1}H NMR (CDCl$_3$) δ 8.63 (s, 2H), 8.01 (s, 1H), 4.82–4.76 (m, 1H), 4.12–4.08 (m, 2H), 3.68 (d, J = 5.0 Hz, 3H), 3.64–3.54 (m, 2H), 3.28 (t, J = 8.3 Hz, 1H), 3.04 (d, J = 9.9 Hz, 1H), 2.89–2.86 (m, 1H), 2.71 (s, 3H), 2.66–2.62 (m, 1H), 2.49–2.27 (m, 3H), 1.97 (t, J = 7.9 Hz, 1H), 1.91–1.83 (m, 2H), 1.19 (d, J = 7.05 Hz, 3H). MS: M + H m/z = 410.2.

6-[(3S,4S)-4-Methyl-1-(pyrimidin-2-ylmethyl)pyrrolidin-3-yl]-1-(tetrahydro-2H-pyran-4-yl)-1,5-dihydro-4H-pyrazolo[3,4-d]pyrimidin-4-one (20). To a solution of 6-[(3S,4S)-4-methylpyrrolidin-3-yl]-1-(tetrahydro-2H-pyran-4-yl)-1H-pyrazolo[3,4-d]pyrimidin-4(5H)-one hydrogen chloride (7.75 g) in dimethylformamide (115 mL) were added iron triflate (900 mg), 2-(chloromethyl)pyrimidine hydrogen chloride (4.5 g), and cesium carbonate (22.2 g), and the reaction mixture was heated at 60 °C for 24 h. The reaction mixture was concentrated onto silica gel and purified by flash chromatography, eluting with 0–15% methanol/ethyl acetate/1% saturated ammonium hydroxide to provide the title compound (6 g). 400 MHz ^{1}H NMR (CDCl$_3$) δ 12.30 (s, 1H), 8.63 (d, J = 5.0, Hz, 2H), 8.03 (s, 1H), 7.20 (d, J = 5.0, Hz, 1H), 4.84–4.79 (m, 1H), 4.30–4.27 (m, 1H), 4.14–4.08 (m, 2H), 3.87–3.82 (m, 1H), 3.63–3.55 (m, 2H), 3.47 (t, J = 7.9 Hz, 1H), 3.29 (d, J = 9.9 Hz, 1H), 2.88–2.86 (m, 1H), 2.60–2.56 (m, 1H), 2.46–2.24 (m, 4H), 1.93–1.84 (m, 2H), 1.24 (t, J = 7.1 Hz, 3H). MS: M + H m/z = 396.2. Anal. Calcd for C$_{20}$H$_{25}$N$_7$O$_2$: C, 60.74%; H, 6.37%; N, 24.79%. Found: C, 60.56%; H, 6.43%; N, 24.61%.

■ ASSOCIATED CONTENT

ⓢ Supporting Information

Experimental procedures for the enzyme assays and pharmacokinetic experiments. This material is available free of charge via the Internet at http://pubs.acs.org.

Accession Codes

Coordinates of the PDE9A crystal structures have been deposited in the Protein Data Base for compound 16 (PDB code 4E90).

■ AUTHOR INFORMATION

Corresponding Author

*Phone: 617-395-0708. Fax: 860-686-0013. E-mail: patrick.r.verhoest@pfizer.com.

Notes

The authors declare no competing financial interest.

■ ABBREVIATIONS USED

PDE, phosphodiesterase; cGMP, cyclic guanosine monophosphate; CNS, central nervous system; SBDD, structure-based drug design; P-gp, P-glycoprotein; LipE, lipophilic ligand efficiency; LE, ligand efficiency; CSF, cerebral spinal fluid; LTP, long-term potentiation

■ REFERENCES

(1) Schmidt, C. J. Phosphodiesterase Inhibitors as Potential Cognition Enhancing Agents. *Curr. Top. Med. Chem.* **2010**, *10*, 222−230.

(2) Beavo, J. A. Cyclic Nucleotide Phosphodiesterases: Functional Implications of Multiple Isoforms. *Phys. Rev.* **1995**, *75*, 725−748.

(3) Setter, S. M.; Iltz, J. L.; Fincham, J. E.; Campbell, R. K.; Baker, D. E. Phosphodiesterase 5 Inhibitors for Erectile Dysfunction. *Ann. Pharmacol.* **2005**, *39*, 1286−1295.

(4) Zewail, A. M.; Newar, M.; Vrtovec, B.; Eastwood, C.; Biswajit, K.; Delgado, R. M. Intravenous Milrinone in Treatment of Advanced Congestive Heart Failure. *Tex. Heart Inst. J.* **2003**, *30*, 109−113.

(5) Boswell-Smith, V; Spina, D. PDE4 Inhibitors as Potential Therapeutic Agents in the Treatment of COPD-Focus on Roflumilast. *Int. J. Chronic Obstruct. Pulm. Dis.* **2007**, *2*, 121−129.

(6) Cote, R. H.; Feng, Q.; Valeriani, B. A. Relative Potency of Various Classes of Phosphodiesterase (PDE) Inhibitors for Rod and Cone Photoreceptor PDE6. *Invest. Ophthalmol.* **2003**, *44*, 1524−1527.

(7) Young, R. A.; Ward, A. Milrinone. A Preliminary Review of Its Pharmacological Properties and Therapeutic Use. *Drugs* **1988**, *36*, 158−192.

(8) Card, G. L.; England, B. P.; Suzuki, Y.; Fong, D.; Powell, B.; Lee, B.; Luu, C.; Tabrizizad, M.; Gillete, S.; Ibrahim, P. N.; Artis, D. R.; Bollag, G.; Milburn, M. V.; Kim, S.; Schlessinger, J.; Zang, K. Y. J. Structural Basis for the Activity of Drugs That Inhibit Phosphodiesterases. *Structure* **2004**, *12*, 2233−2247.

(9) Menniti, F. S.; Faraci, S. W.; Schmidt, C. J. Phosphodiesterases in the CNS: Targets for Drug Development. *Nat. Rev. Drug Discovery* **2006**, *5*, 660−670.

(10) Chappie, T. A.; Humphrey, J. M.; Allen, M. P.; Estep, K. G.; Fox, C. B.; Lebel, L. A.; Liras, S.; Marr, E. S.; Menniti, F. S.; Pandit, J.; Schmidt, C. J.; Tu, M.; Williams, R. D.; Yang, F. V. Discovery of a Series of 6,7-Dimethoxy-4-pyrrolidylquinazoline PDE10A Inhibitors. *J. Med. Chem.* **2007**, *50*, 182−185.

(11) Verhoest, P. R.; Chapin, D. S.; Corman, M.; Fonseca, K.; Harms, J. F.; Hou, X.; Marr, E. S.; Menniti, F. S.; Nelson, F.; O'Connor, R.; Pandit, J.; Proulx-LaFrance, C.; Schmidt, A. W.; Schmidt, C. J.; Suiciak, J. A.; Liras, S. Discovery of a Novel Class of PDE10A Inhibitors and Identification of Clinical Candidate 2-[4-(1-Methyl-4-pyridin-4-yl-1*H*-pyrazol-3-yl)phenoxylmethyl]quinoline (PF-2545920) for the Treatment of Schizophrenia. *J. Med. Chem.* **2009**, *52*, 5188−5196.

(12) Lu, Y.; Kandel, E., R.; Hawkins, R. D. Nitric Oxide Signaling Contributes to Late-Phase LTP and CREB Phosphorylation in the Hippocampus. *J. Neurosci.* **1999**, *19*, 10250−10261.

(13) Puzzo, D.; Vitolo, O.; Fabrizio, T.; Jacob, J. P.; Palmeri, A.; Arancio, O. Amyloid-beta Peptide Inhibits Activation of the Nitric Oxide/cGMP/cAMP Responsive Element-Binding Protein Pathway during Hippocampal Synaptic Plasticity. *J. Neurosci.* **2005**, *25*, 6887−6897.

(14) Fisher, D. A.; Smith, J. F.; Pillar, J. S.; Denis, S. H.; Cheng, J. B. Isolation and Characterization of PDE9A, a Novel Human cGMP-Specific Phosphodiesterase. *J. Biol. Chem.* **1998**, *25*, 15559−15564.

(15) Andreeva, S. G.; Dikkes, P.; Epstein, P. M.; Rosenberg, P. A. Expression of cGMP-Specific Phosphodiesterase 9A mRNA in the Rat Brain. *J. Neurosci.* **2001**, *15*, 9068−9076.

(16) Van Der Staay, F. J.; Rutten, K.; Barfacker, L.; DeVry, J.; Erb, C.; Schroder, H. H.; Hendrix, M. The Novel Selective PDE9 Inhibitor BAY 73-6691 Improves Learning and Memory in Rodents. *Neuropharmacology* **2008**, *55*, 908−918.

(17) Verhoest, P. R.; Proulx-Lafrance, C.; Corman, M.; Chenard, L.; Helal, C. J.; Hou, X.; Kleiman, R.; Liu, S.; Marr, E.; Menniti, F. S.; Schmidt, C. J.; Vanase-Frawley, M.; Schmidt, A. W.; Williams, R. D.; Nelson, F. R.; Fonseca, K. R.; Liras, S. Identification of a Brain Penetrant PDE9A Inhibitor Utilizing Prospective Design and Chemical Enablement as a Rapid Lead Optimization Strategy. *J. Med. Chem.* **2009**, *52*, 7946−7949.

(18) Whalen, K.; Gobey, J.; Janiszewski, J. A. Centralized Approach to Tandem Mass Spectrometry Method Development for High-Throughput ADME Screening. *Rapid Commun. Mass Spectrom.* **2006**, *20*, 1497−1503.

(19) Kuntz, I. D.; Chen, K.; Sharp, K. A.; Kollman, P. A. The Maximal Affinity of Ligands. *Proc. Natl. Acad. Sci. U.S.A.* **1999**, *96*, 9997−10002.

(20) Wager, T. T.; Chandrasekaran, R. Y.; Hou, X.; Troutman, M. D.; Verhoest, P. R.; Villalobos, A.; Will, Y. Defining Desirable Central Nervous System Drug Space through the Alignment of Molecular Properties, in Vitro ADME, and Safety Attributes. *ACS Chem. Neurosci.* **2010**, *1*, 420−434.

(21) Feng, B; Mills, J. B.; Davidson, R. E.; Mireles, R. J.; Janiszewski, J. S.; Troutman, M. D.; de Morais, S. M. In Vitro P-Glycoprotein Assays To Predict the in Vivo Interactions of P-Glycoprotein with Drugs in the Central Nervous System. *Drug Metab. Dispos.* **2008**, *36*, 268−275.

(22) Obach, R. S. Prediction of Human Clearance of Twenty-Nine Drugs from Hepatic Microsomal Intrinsic Clearance Data: An Examination of in Vitro Half-Life Approach and Nonspecific Binding to Microsomes. *Drug. Metab. Dispos.* **1999**, *27*, 1350−1359.

(23) Obach, S. R.; Baxter, J. G.; Liston, T. E.; Silber, B. M.; Jones, B. C.; MacIntyre, F.; Rance, D. J.; Wastall, P. The Prediction of Human Pharmacokinetic Parameters from Preclinical and in Vitro Metabolism Data. *J. Pharmacol. Exp. Ther.* **1997**, *283*, 46−58.

(24) Kleiman, R. J.; Chapin, D. S.; Christoffersen, C.; Freeman, J.; Fonseca, K. R.; Geoghegan, K. F.; Grimwood, S.; Guanowsky, V.; Hajos, M.; Harms, J. F.; Helal, C. J.; Hoffman, W. E.; Kocan, G. P.; Majchrzak, M.; McGinnis, D.; McLean, S.; Menniti, F. S.; Nelson, F.; Roof, R.; Schmidt, A. W.; Seymour, P. A.; Stephenson, D. T.; Tingley, F. D.; Vanase-Frawley, M.; Verhoest, P. R.; Schmidt, C. J. Phosphodiesterase 9A Regulates Central cGMP and Modulates Responses to Cholinergic and Monoaminergic Perturbation in Vivo. *J. Pharmacol. Exp. Ther.* **2012**, *341*, 1−14.

(25) Vardigan, J. D.; Convero, A.; Hutson, P. H.; Uslaner, J. M. Selective Phosphodiesterase 9 Inhibitor PF-04447943 Attenuates a Scapolamine-Induced Deficits in a Novel Rodent Attenuation Task. *J. Neurogenet.* **2011**, *25*, 120−126.

(26) Hutson, P. H.; Finger, E. N.; Magliaro, B. C.; Smith, S. M.; Converso, A.; Sanderson, P. E.; Mullins, D.; Hyde, L. A.; Eschle, B. K.; Turnbull, Z.; Sloan, H.; Guzzi, M.; Zhang, X.; Wang, A.; Rindgen, D.; Mazzola, R.; Vivian, J. A.; Eddins, D.; Uslaner, J. M.; Bednar, R.; Gambone, C.; Le-Mari, W.; Marino, M. J.; Sachs, N.; Xu, G.; Parmentier-Batteur, S. The Selective Phosphodiesterase 9 (PDE9) Inhibitor PF-04447943 (6-[(3*S*,4*S*)-4-methyl-1-(pyrimidin-2-ylmethyl)pyrrolidin-3-yl]-1-(tetrahydro-2*H*-pyran-4-yl)-1,5-dihydro-4*H*-pyrazolo[3,4-*d*]pyrimidin-4-one) Enhances Synaptic Plasticity and Cognitive Function in Rodents. *Neuropharmacology* **2011**, *61*, 665−667.

(27) Kleiman, R. J.; Lanz, T. A.; Finley, J. E.; Bove, S. E.; Majchrzak, M. J.; Becker, S. L.; Carvajal-Gonzales, S.; Kuhn, A. M.; Wood, K. M.; Mariga, A.; Nelson, F. R.; Verhoest, P. R.; Seymour, P. A; Stephenson, D. T. Dendritic Spine Density Deficits in the Hippocampal CA1 Region of Young Tg2576 Mice Are Ameliorated with the PDE9A Inhibitor PF-04447943. *Alzheimer's Dementia* **2010**, *6*, S563−S564.

(28) Wager, T. T.; Hou, X.; Verhoest, P. R.; Villalobos, A. Moving beyond Rules: The Development of a Central Nervous System Multiparameter Optimization (CNS MPO) Approach To Enable Alignment of Druglike Properties. *ACS Chem. Neurosci.* **2010**, *1*, 435−449.

(29) Evans, R. M.; Nicholas, T.; Le, V.; Qiu, R.; Martin, W.; Martin, D.; Styren, S.; Fullerton, T.; Schwam, E. Safety and Pharmacokinetics

of PF-04447943, a PDE9A Inhibitor, in Single and Mulitple Dose Phase 1 Studies in Healthy Volunteers. *Alzheimer's Dementia* **2010**, *6*, S135.

(30) Nicholas, T.; Evans, R.; Styren, S.; Qui, R.; Wang, E. Q.; Nelson, F.; Le, V.; Grimwood, S; Christoffersen, C.; Banerjee, S.; Corrigan, B.; Kocan, G.; Geoghegan, K.; Carrieri, C.; Raha, N.; Verhoest, P.; Soares, H. PF-04447943, a Novel PDE9A Inhibitor, Increases cGMP Levels in Cerebrospinal Fluid: Translation from Non-Clinical Species to Healthy Human Volunteers. *Alzheimer's Dementia* **2009**, *5*, P330−P331.